# **Analysis of the Water Permeability of Linde Type A Zeolites in Reverse Osmosis**

Pinar Cay-Durgun, Shawn G. Fink, Andrew Shabilla, Huidan Yin, Kenji A. Sasaki, and Mary Laura Lind

### **QUERY SHEET**

This page lists questions we have about your paper. The numbers displayed at left can be found in the text of the paper for reference. In addition, please review your paper as a whole for correctness.

There are no Editor Queries for this paper.

### TABLE OF CONTENTS LISTING

The table of contents for the journal will list your paper exactly as it appears below:

Analysis of the Water Permeability of Linde Type A Zeolites in Reverse Osmosis Pinar Cay-Durgun, Shawn G. Fink, Andrew Shabilla, Huidan Yin, Kenji A. Sasaki, and Mary Laura Lind DOI: 10.1080/01496395.2014.946147



40

45

50

55

60

65

70

## Analysis of the Water Permeability of Linde Type A Zeolites in Reverse Osmosis

### Pinar Cay-Durgun, Shawn G. Fink, Andrew Shabilla, Huidan Yin, Kenji A. Sasaki, and Mary Laura Lind

5 School for Engineering of Matter, Transport, and Energy, Arizona State University, Tempe, Arizona, USA

In this paper, we apply the Hagan-Poiseuille Model and the resistance model to perform original analysis of previous experimental studies of water transport through polycrystalline Linde Type A (LTA) zeolite membranes and nanocomposite polymer/LTA membranes. From our analysis we estimate the intrinsic water permeability of LTA zeolites and the zeolite/polymer interface. We find that the permeability of a single LTA crystal is significantly greater than the intrinsic permeability of a commercial seawater reverse osmosis membrane or a commercial cellulose-acetate forward osmosis membrane.

**Keywords** zeolite; LTA; molecular sieve; reverse osmosis; hydraulic permeability; permeance; nanocomposite

### **INTRODUCTION**

15

20

30

35

Purification of water from impaired sources (e.g., saline waters and wastewaters) is critical to human survival and environmental sustainability (1). Reverse Osmosis (RO) is a leading industrial technique for generating high purity water; RO offers relatively low energy consumption compared to techniques such as multistage flash (MSF) and multiple-effect distillation (MED) (2). To achieve a sustainable water future, however, the RO method requires the development of a new generation of higher performance membranes.

Conventional RO membranes are dense, non-porous, polymeric membranes, which operate via a solution-diffusion mechanism (3, 4). Dense membranes that separate via the solution-diffusion mechanism are ubiquitous in environmental and energy separations (e.g., water purification (5), separation of organics from water (6), and methane purification (7)). However, there are two challenges facing dense polymeric membranes for water separation:

2. many of the polymers suitable for the desired separation are intolerant of harsh environments (extreme pHs, temperatures, oxidizing conditions).

Molecular sieve materials (e.g., zeolites, metal-organic-frameworks, and zeolite imidazolate frameworks), though expensive to fabricate as continuous thin film membranes (11, 12), may offer solutions to these two challenges. In gas separations, molecular sieves exhibit performance that exceeds the polymeric upper bound (13). Molecular sieves, because of their high inorganic content, are robust enough to withstand extreme environments.

Polycrystalline Linde Type A (LTA) zeolites are extremely hydrophilic and have a central pore of  $\sim$ 4.2 Å (14). Single LTA zeolite nanoparticles have exhibited high rejection of small molecules in gas separations (15). These properties give zeolites great potential for aqueous membrane separation applications.

In a thorough review of the literature, we found limited experimental research on hydraulic permeation of aqueous solutions through polycrystalline LTA membranes, and no experimental reports on hydraulic permeation through single crystal LTA membranes. Cui et al. grew polycrystalline LTA zeolite membranes on the inner surfaces of macroporous alumina tubes (16). By varying the growth time, they were able to change both the overall thickness of the LTA membrane as well as the inter-particle pore size (the spacing between single-crystal grains); this resulted in three distinct membranes with different characteristic inter-particle pore sizes. Cui et al. used gas permeation, bubble point, imaging, and cross-flow filtration to determine the membrane pore size, thickness, water flux, and oil rejection; we present a summary of their results in TABLE 1 (16).

Mixed-matrix-membranes (MMMs) are a desirable alternative to polycrystalline molecular sieve membranes, as they are easier to synthesize and have potential to be scaled up more

<sup>1.</sup> the overall performance has an upper bound, as a tradeoff exists between membrane permeability and selectivity (8–10), and

Received 8 May 2014: accepted 15 July 2014.

Address correspondence to Mary Laura Lind, School for Engineering of Matter, Transport, and Energy, Arizona State University, Tempe, AZ, USA 85287. E-mail: mllind@asu.edu

P. CAY-DURGUN ET AL.

TABLE 1

Membrane characteristics and experimental performance results data reproduced from Cui et al. polycrystalline LTA zeolite membranes coated on ceramic supports (16)

Cui et al.	Coating Thickness (µm)	Interfacial Pore Size (µm)	Pure Water Permeability (µm s <sup>-1</sup> MPa <sup>-1</sup> )	Oil Rejection (%)
Ceramic Support	0	2.1	$611.1 (\pm 61.1)$	$89.77 (\pm 1.8)$
NaA1	6	1.2	$472.2 (\pm 47.2)$	$98.83 (\pm 0.99)$
NaA2	10	0.4	$50.00 (\pm 5.00)$	$99.42 (\pm 0.99)$
NaA3	12	0.2	$27.78 (\pm 2.78)$	n/a

readily (13). MMMs incorporate micron-sized particles (molecular sieves, pure metals, and other inorganic solids) into thick polymeric films, often demonstrating improved separation performance properties compared to pure polymeric membranes (17–20). A recent trend in MMM research is to incorporate inorganic, nanoscale, molecular sieve particles into thin polymeric films (21–23).

75

80

85

90

95

100

105

110

In 2007, Jeong et al. incorporated single-crystal LTA zeolite nanoparticles into polyamide thin films for reverse osmosis (24). In these experiments, they incorporated two types of zeolites: "pore-filled" and "pore-open." In "pore-filled" zeolites, the templating agent remained inside the central pores of the crystal structure, while in "pore-open" zeolites they removed the templating agent from the pores. Jeong's use of pore-filled and pore-open zeolites is an essential part of our analysis, allowing us to separate permeation through the zeolite crystal pores from permeation through the membrane and the polymer-zeolite interface.

The separation performance of an RO membrane is a function of the rate at which water moves through it. In order to maximize the potential of new membrane technologies, it is necessary to understand the nature of water transport through the membrane elements. The exact mechanism of hydraulic transport through the pores of molecular sieve materials remains an open scientific question (25). One theory suggests that the overall diffusion of gases is actually three separate mechanisms: bulk diffusion, Knudsen diffusion, and surface diffusion (25). In addition, the dominant transport mechanism depends on the pore size. In bulk diffusion, moleculemolecule collisions transport the fluid from the bulk to the pore. Within large pores, molecule-wall collisions dominate, typical of Knudsen diffusion. Finally, in very small pores, surface diffusion dominates, as molecules are adsorbed to the pore wall.

Recently, Cohen et al. performed molecular dynamics simulations for pressure-driven water transport through bulk and thin film membranes of LTA zeolite (26). They found that simulated fluxes through a thin film zeolite membrane were lower than the experimentally reported fluxes of pure polyamide thin film membranes (27). On the other hand, with the addition of LTA zeolite into polyamide matrix, water flux usually increases

(24, 28, 29). Therefore, Cohen et al. (26) hypothesized that water may preferentially flow around the zeolite particles and not through the zeolite pores. In our work, instead of modeling transport mechanisms, we focus on quantifying the water flux through single crystal zeolites, in polycrystalline zeolite, and mixed matrix membranes, whose performance has been evaluated experimentally.

120

125

135

140

145

150

Determining the intrinsic properties of LTA zeolites, the polymer, and the zeolite/polymer interface is critical to the investigation of MMMs for RO applications. Performance models allow us to design and create improved membranes and explain deviations from ideal behavior. However, quantitative models are not feasible without reliable physical property data.

In this paper we present an original analysis of experimental results reported by Cui et al. (16) and Jeong et al. (24) (summarized in TABLE 1 and TABLE 2). We apply two models to these experimental results to estimate the intrinsic permeability of single crystal LTA zeolites, the zeolite/polymer interface, and to determine effective permeability in the polyamide mixed matrix system. Our paper is the first analysis quantifying the experimental water transport through single crystal LTA zeolites estimated from polycrystalline zeolite and mixed matrix membranes.

### **EXPERIMENTAL METHODS**

We applied the Hagen-Poiseuille Model and the resistance model to analyze the data from two previously published works: polycrystalline zeolite membranes (16) and mixed matrix zeolite-in-polymer membranes (24). We separate overall membrane flux into flux through each constituent phase.

### **Definitions and Calculation of Membrane Transport Coefficients**

In pressure driven membrane processes, the volumetric flux of water,  $J_{water}$  (m/s), measures the rate of permeation through the membrane. Experimentally, this water flux is calculated by measuring the volume of water that passes through a specific area of membrane during a defined time.

190

200

205

210

TABLE 2

Summary of membrane characteristics and experimental reverse osmosis performance results from Jeong et al. mixed matrix membranes (24). These membranes consist of a polyamide rejection layer (50-200 nm) cast with zeolite particles (100 nm) on polysulfone/polyester composite support

Membrane	Zeolite	Nominal Zeolite Content (w/v %)	NaCl Permeance (2000 ppm) $(\mu m s^{-1} MPa^{-1})$	NaCl Rejection (2000 ppm) (%)
J1	None	0	$2.09 (\pm .0999)$	93.38 (± 1.14)
J2	Pore-open	0.004	$2.13 (\pm .0998)$	$93.84 (\pm 1.14)$
J3	Pore-open	0.01	$2.48 (\pm .0809)$	$94.06 (\pm 1.15)$
J4	Pore-open	0.04	$2.86 (\pm .201)$	$94.29 (\pm 1.15)$
J5	Pore-open	0.1	$3.16 (\pm .100)$	$93.84 (\pm 1.14)$
J6	Pore-open	0.4	$3.77 (\pm .311)$	$93.84 (\pm 1.14)$
J7	Pore-filled	0.04	$2.51 (\pm .109)$	n/a

Within the literature on pressure driven liquid separations, the terms permeance and permeability have been used interchangeably to refer to the A parameter (often called the water permeability coefficient) with units of  $[\mu m \ s^{-1} \ MPa^{-1}]$  (4, 30–34). In the solution diffusion model, describing transport through dense polymeric membranes (4, 30), the permeance (32) ( $A \ [\mu m \ s^{-1} \ MPa^{-1}]$ ) of a component through a membrane is the product of the diffusivity solubility, and thickness of that component within the membrane (30). (1) presents the relationship between the permeance ( $A \ [\mu m \ s^{-1} \ MPa^{-1}]$ ), the measured flux ( $J \ [m/s]$ ), and the driving force for transport in reverse osmosis. In RO, the driving force for transport is the difference between the applied pressure ( $\delta P \ [Pa]$ ) and the osmotic pressure of the solution ( $\Delta \pi \ [Pa]$ ) to be purified.

155

160

165

170

175

180

$$J = A \left( \Delta P - \Delta \pi \right) \tag{1}$$

A is often used to compare different membranes of the same general structure (e.g., commercial thin film composites) that have been produced by different manufacturers (31, 35–37).

However, A depends on membrane thickness. In this paper, we analyze membranes that have thicknesses separated by two orders of magnitude. Rather than using permeance, we find for pure polyamide thin film membranes, it more meaningful to use permeability (8) (P' [ $\mu$ m² s<sup>-1</sup> MPa<sup>-1</sup>]), which is permeance normalized by membrane thickness. The permeability is defined by (2) in terms of permeance [A], where  $\Delta x$  is the thickness of the membrane.

$$P' = A \cdot \Delta x \tag{2}$$

Within this paper, our usage of the terms permeance and permeability follows the conventions used in gas transport theories. The permeability describes an intensive property of a membrane (independent of membrane thickness), while permeance describes an extensive property (dependent on membrane

thickness). Permeability and permeance are frequently used to compare membrane performance in gas separations (19, 38–42). In gas separations, permeability is reported in [mol m<sup>-1</sup> s<sup>-1</sup> Pa<sup>-1</sup>] which is equivalent to our usage of [ $\mu$ m<sup>2</sup> s<sup>-1</sup> MPa<sup>-1</sup>] in this paper.

### Theoretical Models Describing Transport through Membranes

We use two models to describe the transport through the porous, polycrystalline zeolite membranes of Cui et al. (16) and through the dense polymeric/zeolite nanocomposite membranes of Jeong et al. (24). We apply the Hagen-Poiseuille model to the data of Cui et al. (16) to determine the permeability of the macroporous alumina tubes coated with polycrystalline zeolites that were described in that work. We then use a resistance model to isolate the properties of the zeolites in nanocomposite MMMs reported by Jeong et al. (24).

### The Hagen-Poiseuille Model

The Hagen-Poiseuille equation describes pressure driven flow of a viscous fluid through a cylindrical pore (30). The Hagen-Poiseuille model presented in (3) has been used in previous analyses of dense polymeric and ceramic membranes (43-45). (3) assumes that a membrane is a collection of uniform cylindrical pores (30). The intergrown crystals synthesized by Cui et al. (16) create polycrystalline membranes that may exhibit a pore structure that deviates from this idealized assumption. However, the Hagen-Poiseuille equation is the best approximation that we can make to analyze the available information. In Eq. (3) the overall flux (J [m/s]) through the membrane is a function of porosity ( $\varepsilon$  [dimensionless]), pore radius (r [m]), viscosity of the liquid ( $\eta$  [Pa·s]), tortuosity of the pores ( $\tau$  [dimensionless]), the thickness of the membrane  $(\Delta x [m])$ , and the pressure difference across the membrane  $(\Delta P [Pa]).$ 

220

225

230

235

$$J = \frac{\varepsilon r^2}{8\eta\tau} \frac{\Delta P}{\Delta x} \tag{3}$$

The Resistance Model

The resistance model describes transport through multiphase or multi-component membranes, such as thin film composites for water and gas separations and has recently been introduced to mixed matrix membranes (46–49). This model treats fluid flow through multi-component membranes as analogous to the flow of current through resistors (47). The resistance (R [s MPa  $\mu$ m<sup>-1</sup>]) of a material is related to the permeance, A, and the permeability, P', as described in (4).

$$R = \frac{1}{A} = \frac{\Delta x}{P'} \tag{4}$$

In the nanocomposite membranes synthesized by Jeong et al. the average diameter of the zeolite nanoparticles is nearly equal to the thickness of the polyamide layer (24). Therefore, we consider the polymer matrix and nanoparticles as parallel resistances. Mathematically, this is represented in (5).

$$\frac{1}{R_{Overall}} = \frac{1 - v}{R_{Polymer}} + \frac{v}{R_{Interface}} + \frac{v}{R_{Zeolite}}$$
 (5)

In (5),  $R_{Overall}$  [s MPa  $\mu$ m<sup>-1</sup>] is the total resistance of the mixed matrix membrane.  $R_{Polymer}$ ,  $R_{Interface}$ , and  $R_{Zeolite}$  are the individual resistances of the polymer matrix, matrix-particle interface, and zeolite particle, respectively. The percent volume of the membrane that is occupied by porous zeolite particles is represented by v [v/v%]. Because of limited data from the original Jeong et al. publication, we assumed v is directly proportional to the nominal zeolite content in the monomer solution of the membranes fabricated by Jeong et al. (24). Additionally, we assumed the zeolites are single, unaggregated particles in the

matrix and the concentration of particles in the the zeolitepolymer interface is the same as the concentration of the zeolite particles in the casting solution.

240

245

250

255

260

265

Application of the Hagen–Poiseuille Model to Polycrystalline Zeolite Membranes

We apply the Hagen-Poiseuille model to the data of Cui et al. (16) to determine the zeolite crystal permeability from the polycrystalline zeolite membranes grown on macroporous alumina tubes described in that work. Figure 1 schematically depicts the two possible pathways for transport of molecules through continuous macroscopic polycrystalline zeolite membranes. The first pathway for transport is the space at the interface between individual zeolite crystals (represented by the dotted line). The second transport pathway runs through the pores of a single zeolite crystal (represented by the solid line). In this analysis, we use the Hagen–Poiseuille model to estimate the flux through the interface. We then subtract the contribution of the flux through the interface from the overall flux to estimate the flux through the zeolite pores. From these flux estimates, using the known applied pressure and membrane thickness, we can calculate the water permeability of a single zeolite crystal.

In order to apply the Hagen–Poiseuille model to the pure zeolite membranes in Cui et al. (16), we made the following simple assumptions:

HP1. The zeolite membranes are continuous and defect-free. That is, the only pathways for transport through the membranes are within single zeolite crystals and at the interface boundaries between different zeolite crystals as depicted in Figure 1. Mathematically this is represented by (6).

$$J_{Total} = J_{Interface} + J_{Zeolite}$$
 (6)

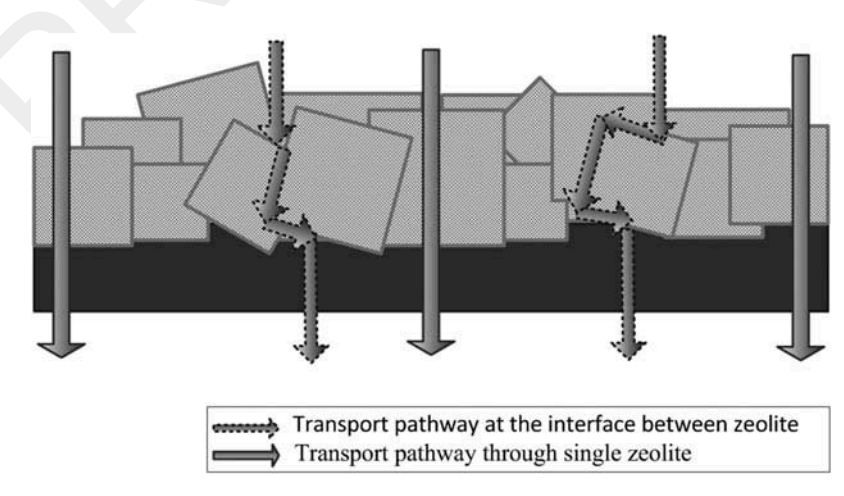


FIG. 1. Representation of zeolite membrane formation on ceramic support of Cui et al. (16) and the possible transport pathways through the zeolite phases.

330

335

345

350

355

360

365

HP2. The interface pathways between the zeolite crystals can be approximated as straight cylinders with a radii indicated by the measured pore size distribution.

This is an idealization of the polycrystalline structure and the fundamental assumption of the Hagen–Poiseuille model. In reality, this assumption eliminates the tortuosity of the interfacial pathway, and will overestimate J<sub>Interface</sub>, the contribution of the interface to total mem-

270

275

280

285

300

305

310

brane flux.

HP3. The tortuosity of the pathways within the zeolite crystals fabricated by Cui et al. is constant (16).

Assumption HP3 is based on the randomness of the zeolite growth; while the actual tortuosity of the membranes is unknown, we assume that it is constant throughout all layers. As such, we use a value of 1.0 in our calculations. With assumption HP3, the final result is independent of the specific tortuosity value used.

HP4. The porosity of the membrane at the interfaces between

crystals (porosities between crystals) is dependent on the characteristic pore radius.

Assumption HP4 is based on the theory that consecutive growth of the zeolites leads to an increase in crystal size, not new nucleation of crystals (50). Therefore, the number of pores remains constant, and the pore size at the crystal grain interface is reduced. Thus, the ratio of porosities between the three membranes reported by Cui et al. (16) (NaA1, NaA2, and NaA3; TABLE 1) can be estimated by the change in area of an interfacial pore.

Cui et al. report experimental information on the flux, the interface pore radius, the applied pressure drop, water viscosity, and membrane thickness for three types of membranes (TABLE 1) (16). We begin by ignoring the contribution of flux through zeolite pores to the overall flux in the first membrane, NaA1. It is likely that the flux through the interfaces between different zeolite crystal grains is much greater than through the zeolite pores, because the interface spacing is significantly larger than the zeolite pores in NaA1 (the experimentally measured interfacial pore size is 1.2 µm while LTA zeolite pores have a diameter of  $\sim$ 4.2 Å (14)). Therefore,  $J_{Total} = J_{Interface} =$  $J_{NaAI}$ . Then using assumption HP3 (tortuosity = 1) we can rearrange (3), the Hagen–Poiseuille model, to solve for the interface porosity (porosities between crystals) of the NaA1 membrane. From this calculated porosity of the NaA1 membrane, we use assumption HP4 to estimate the porosity of the NaA2 and NaA3 membranes using the reported pore radius (r [m]) and the following relationship (7).

$$\varepsilon = \varepsilon_{NaA1} \cdot \frac{r^2}{r_{NaA1}^2} \tag{7}$$

After we estimate the porosity of the membranes, we substitute these values into (3) to solve for the interface flux. Then, we subtract this estimated interface flux from the reported overall flux, as indicated by (6), to yield the flux through the

zeolite particles,  $J_{Zeolite}$ . We then use this value for  $J_{Zeolite}$  in (1) to find the permeance of the zeolite crystals. Because Cui et al. reported the pure water flux,  $\pi$  (the osmotic pressure) is zero (16). Finally, we calculate the zeolite crystal permeability with (2) using the calculated zeolite permeance and reported membrane thickness.

Once we determined a solution for zeolite crystal permeability, we can return to the calculation of porosity in membrane NaA1. This time we do not ignore the zeolite contribution. Then we iterate through the calculation steps until the estimated zeolite crystal permeability used in NaA1 converges with the estimated zeolite crystal permeability calculated from membrane NaA3.

Application of the Resistance Model to Mixed Matrix Membranes

We use a resistance model to isolate the properties of the zeolite in nanocomposite MMMs. The membranes fabricated by Jeong et al. (24) offer a unique simplification of the traditional Maxwell-type resistance analysis (49), because they used particles with dimensions similar to the thickness of the selective polyamide matrix. This allows us to treat the membranes as multiple resistances in parallel. However, because of the known rough morphology of polyamide films (51) (often described as "hill and valley") it is possible that not all zeolites will be exposed at the membrane surface. As such, it is expected that our effective estimate of the zeolite crystal permeability within the MMM will be lower than zeolites in a pure zeolite film.

Figure 2 schematically depicts the three possible independent pathways for transport through the Jeong et al. (24) nanocomposite membranes: through the bulk polymer matrix, through the matrix-particle interface, and through the nanoparticles themselves. Estimating the permeability of the bulk matrix and matrix-particle interface allows for us to isolate the zeolite crystal permeability. Jeong et al. created membranes with three types of selective layers on the traditional polyester/polysulfone composite RO support:

- 1. a thin polyamide membrane.
- 2. a polyamide MMM with pore-open zeolites, and
- 3. a polyamide MMM with pore-filled zeolites. (24) Jeong et al. measured pure water flux and NaCl rejection of these three types of membranes (24). In order to apply the resistance model to analyze their data we have made the following assumptions:

RM1. The pure polymer and nanocomposite membranes are continuous and defect-free. Under this assumption, the only pathways for transport through the membranes are through the polymer, through the matrix-particle interface, and through the zeolite particle. The high sodium chloride rejection rates of the Jeong et al. (24) membranes support this assumption. And, following RM1, all transport must pass through the bulk polymer, the polymer zeolite interface, or the zeolites.

380

385

390

395

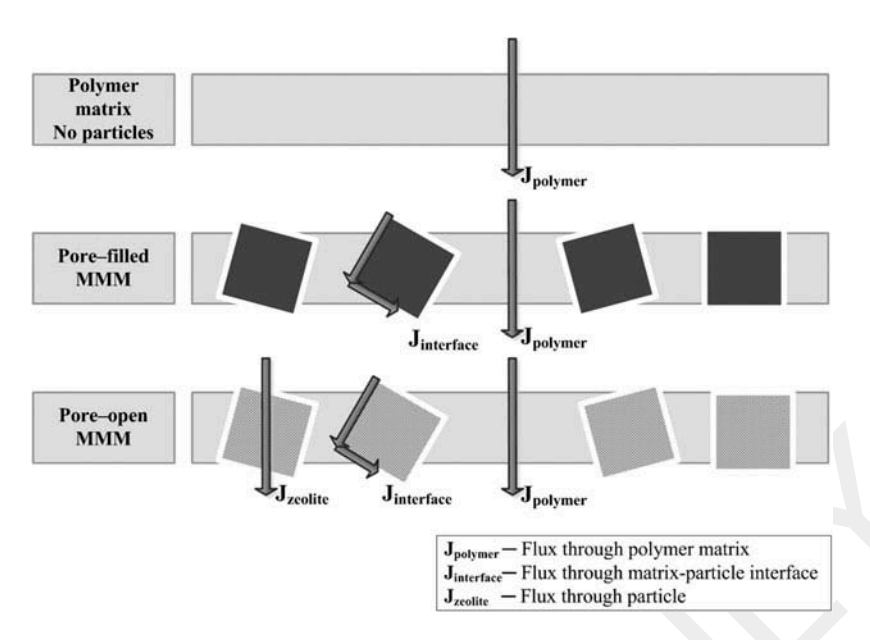


FIG. 2. Representation of transport pathways through rejection layer of mixed matrix membranes (MMM) in Jeong et al. (24). This consists of a polyamide rejection layer (50-200 nm) with zeolite particles (100nm) on a polysulfone/polyester composite support.

370 RM2. The inverse of the total resistance (R<sub>Overall</sub>) is equal to the sum of inverses of the resistance through each phase as described previously in (5).

Each of the three phases has an intrinsic permeability and a corresponding resistance (determined by (4).

ity and a corresponding resistance (determined by (4). Simultaneous, independent flow through these phases leads to (5), analogous to electric current flow.

RM3. The permeability of the matrix-particle interface is independent of the state of the zeolite pores (i.e., whether the zeolite pores are open or filled).

The pores of the pore-filled zeolites retain the templating agent, around which the zeolites nucleate and grow. We assume that the concentration of the templating agent at the zeolite particle interface is negligible.

RM4. Incorporation of zeolites does not change the permeability of the bulk polymer. Assumption RM4 is based on the very low zeolite loadings used by Jeong et al. (24) At low values of zeolite loading, there should be no effect on the bulk polymer phase.

RM5. RM5. The weights of the zeolite resistance and of the interface resistance are proportional to the zeolite particles in the monomer solution.

As noted by Jeong et al. (24), nanoparticles of LTA zeolites were dispersed in the membrane casting solutions by extensive sonication of the solution, this implies (but does not confirm) assumption RM5.

RM6. RM6. The zeolite nanoparticles are single crystals.

This analysis does not account for aggregation of particles or polycrystalline particles.

Jeong et al. present the total permeance of each membrane (24), we have summarized these results and membrane characteristics in TABLE 2. We applied (4) to convert the reported Jeong et al. permeance (24) into permeability. For the pure polymer membrane, J1, v (the concentration of particles in the membrane) is zero and the total resistance is equal to the polymer resistance; R<sub>Polymer</sub> is easily solved for. Next, we isolate the interface resistance using data from J7, the pore-filled zeolite membrane. In the calculation for J7 we neglect the  $v/R_{Zeolite}$ term because the zeolite pores in J7 are filled with templating agent and R<sub>Polymer</sub> is already known from the previous calculation. Next we solve for R<sub>Interface</sub> with (5). Then, we hold the calculated values of R<sub>Polymer</sub> and R<sub>Interface</sub> constant for each subsequent membrane calculation, following assumption RM4. With R<sub>Overall</sub> calculated from the data, a rearrangement of (5) to (8) yields a value for the resistance of the zeolite particles in membranes J2-J6.

$$R_{Zeolite} = \frac{v}{\frac{1}{R_{Overall}} - \frac{1 - v}{R_{Polymer}} - \frac{v}{R_{Interface}}}$$
(8)

400

405

410

415

420

With a solution for  $R_{Zeolite}$  determined and the membrane thickness known, the zeolite crystal permeability, P', is found by rearranging (4).

#### **RESULTS AND DISCUSSION**

TABLE 3 presents the permeabilities of LTA zeolite crystals calculated by the above-described analyses of the data collected

465

470

480

485

TABLE 3
Calculated values of permeability of LTA zeolites and polyamide determined from Hagen-Poiseuille analysis on Cui et al.

(16) and Resistance Model of Jeong et al. (24)

	M	Permeability (μm <sup>2</sup> s <sup>-1</sup> MPa <sup>-1</sup> )	
LTA Zeolite	Cui et al.	NaA2	471 (± 115)
		NaA3	$331 (\pm 81)$
	Jeong et al	J2, v/v% = 0.004	$-9.7 (\pm 266)$
		J3, v/v% = 0.01	$261 (\pm 97)$
		J4, v/v% = 0.040	$81 (\pm 41)$
		J5, v/v% = 0.100	$2.4 (\pm 27)$
		J6, v/v% = 0.400	$-56 (\pm 30)$
LTA-PA Interface	Jeong et al.	J7, v/v% = 0.040	$95 (\pm 28)$
Polyamide	Jeong et al. TFC	J1, no zeolite	$0.21 (\pm .011)$
	Commercial TFC	SW30XLE, no zeolite	$0.19 (\pm .033)$

by Cui et al.(16) and Jeong et al. (24) The Hagen–Poiseuille analysis of the polycrystalline zeolite membranes yielded single crystal LTA permeability estimates of 471 ( $\pm$  115) and 331 ( $\pm$  81) [ $\mu m^2$  s $^{-1}$  MPa $^{-1}$ ]. The resistance model analysis of Jeong et al.'s pure polyamide and LTA/polyamide thin film nanocomposite membranes (24) yielded a zeolite/polymer interface permeability estimate of 95 ( $\pm$  28) [ $\mu m^2$  s $^{-1}$  MPa $^{-1}$ ] (calculated from J7 – the pore-filled membrane) and LTA zeolite crystal permeabilites ranging from -56 to 261 [ $\mu m^2$  s $^{-1}$  MPa $^{-1}$ ].

425

430

435

440

445

450

455

In comparison, the permeability of the pure polyamide membrane synthesized by Jeong et al. is  $0.21 \, [\mu m^2 \, s^{-1} \, MPa^{-1}] \, (24)$ , which is very near to the intrinsic permeability of  $0.19 \, [\mu m^2 \, s^{-1} \, MPa^{-1}]$  reported for a commercial sea water membrane (38).

Using samples J4 and J7, which have the same loading of pore-open and pore-filled zeolites, we estimate the zeolite/polyamide interface permeability to be slightly higher than the zeolite permeability. Our analysis indicates that there is preferential flow through the zeolites within the membrane; however, the actual flow appears to be a combination of flow both through and around the zeolite.

The difference between the two values of zeolite crystal permeability that we calculated by the Hagen-Poiseuille method for the polycrystalline membranes of Cui et al. (16) is likely a result of assumption HP4, that the porosity of the polycrystalline membranes is dependent on the characteristic pore radius. However, assumption HP4 is the best estimation of the porosity that we can make from the available information. Experimental analysis of membrane porosity would have eliminated this assumption and the associated error from the calculations. The calculated porosities of NaA1 and NaA2 have a large effect on the calculated zeolite crystal permeability, because of their apparent defects, as seen with the calculation in (7). The porosity of membrane NaA3 has little effect on

the zeolite crystal permeability calculated for NaA3, because experimentally NaA3 has minimal defects (as indicated by its high oil rejection). Therefore, we consider the zeolite crystal permeability calculated from NaA3, 331 ( $\pm$  81) [ $\mu$ m<sup>2</sup> s<sup>-1</sup> MPa<sup>-1</sup>], to be the closest to the actual value.

We hypothesize that the wide range of zeolite crystal permeability estimates resulting from our analysis of Jeong et al.'s membranes (24) may occur for four reasons:

- 1. our assumption RM5 is incorrect, introducing the possibility that the nominal zeolite content of the casting solution is not equal to actual zeolite content of the membrane
- 2. some zeolite particles are partially covered with polymer
- 3. the mathematical accuracy of the model is limited by low zeolite loadings, and
- 4. there may be aggregation of the nanoparticles.

First, Jeong et al. did not experimentally quantify the amount of zeolites in the final membrane, they only reported the nominal loading of zeolites in the casting solution (24). Therefore, it is not known how the concentration of zeolite particles in solution affects the concentration of zeolites in the film. Additionally, it is also unclear how diffusion and buoyancy mechanisms affect zeolite concentration at the interface during the interfacial polymerization of the polyamide film.

Second, it is possible that a region of the polyamide polymer encases the zeolite particle that may further increase resistance. A thin polymer encasing could explain why our calculated zeolite crystal permeabilities decreased with increased zeolite loading. Assumption RM2 and (5) are based on a membrane with equal thickness of polymer and zeolite particle. In reality, a thin polymer layer could exist not only between particles, but also above and below. Thin layers of polymer result in a decrease in accessibility of the particle and a lower effective zeolite crystal permeability of the particle.

P. CAY-DURGUN ET AL.

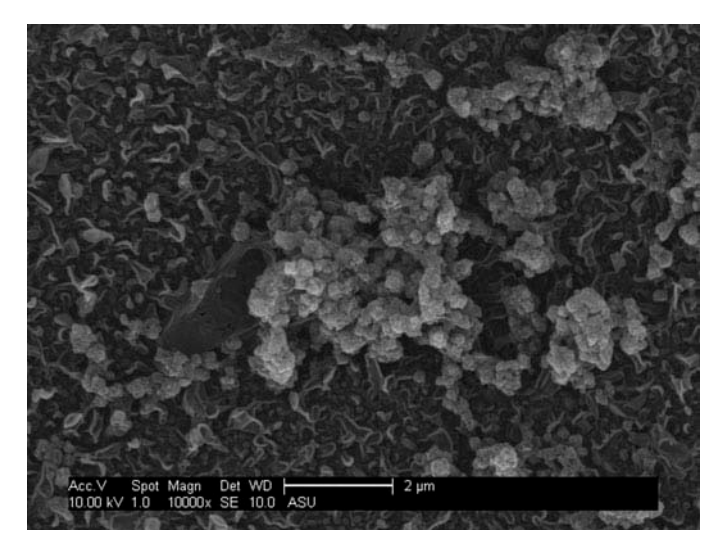


FIG. 3. Aggregate of 100 nm LTA Zeolites on the surface of a LTA/polyamide membrane synthesized in our lab according to the method published in Lind et al. (28) using a nominal loading of .01 wt% LTA zeolites in casting solution.

Third, for nanoparticles content values lower than value of thickness of the membrane active layer square, the accuracy of the model is limited, which can be attributed to the propagation of error. For this reason, the resistance model may not be appropriate for low zeolite loadings (< 0.01 w/v%) in this particular analysis.

490

495

500

505

510

515

520

Fourth, if zeolite particles aggregate in the membrane, assumption RM6 is incorrect. At low zeolite loadings, <0.01 w/v%, the degree of particle aggregation may be minimized, however likely still exists based on the synthesis method used by Jeong et al. (24). In this synthesis of polyamide/LTA nanocomposites the extremely hydrophilic LTA particles are dispersed into a hydrophobic (nonpolar) organic solution; therefore, it is thermodynamically favorable for these hydrophilic particles to aggregate, in order to minimize interfacial free energy. As nanoparticle aggregation increases in the real membrane, our use of an idealized resistances-in-parallel model becomes less applicable. The flow path through the aggregated zeolites across the membrane becomes longer, increasing the resistance to flow. Figure 3 presents scanning electron microscope images of LTA aggregation in polyamide/LTA membranes synthesized in our lab; we synthesized these membranes based on a slightly modified version of the method used by Jeong et al. (24, 28, 29). Dong et al. also reported aggregation of LTA particles in LTA zeolite/polyamide membranes (52).

Since the probability of aggregation increases with zeolite loading, the membrane may have lower concentration of effective nanopaticles in the matrix than the amount nanoparticles in the casting solutions. In addition, because of the limited experimental data, for each loading, we used the same value of interface permeability, which we calculated from the pore-filled membrane, to estimate zeolite permeability. On the other hand,

we have the measured data for the total permeability of membranes for each loading. Therefore, for zeolite loadings higher than the pore-filled membrane content, the model may underestimate the crystal permeability to compensate overestimated effective zeolite content. This may explain the estimated negative zeolite permeability values for membranes J5 and J6. This indicates that our analysis has an upper limit which is set by the highest available pore-filled zeolite membrane data. For our particular case, this occurs to be zeolite contents higher than > 0.04 w/v%.

These theories explain the negative values of zeolite crystal permeability that we calculated by applying the resistance model to Jeong et al.'s LTA/polyamide nanocomposite membranes (24).

530

540

545

550

555

560

565

570

In summary, we believe that the resistance model analysis only applies for a limited range of zeolite loadings. Also, we can clearly estimate the zeolite/polymer interface permeability from the pore-filled zeolites (membranes J7). Therefore, we are confident that the zeolite permeability estimate from the pore-open membrane (J4), which is 81 ( $\pm$  41) [ $\mu$ m<sup>2</sup> s<sup>-1</sup> MPa<sup>-1</sup>], with the same nominal zeolite content as the pore-filled membrane (J7), should be most representative of the actual permeability for a LTA single crystal calculated through the resistance model.

### **CONCLUSIONS**

MMMs continue to be investigated for a number of separation applications (53, 54). They have recently demonstrated improved separation performance over pure polymeric reverse osmosis membranes (24, 27–29). Isolation of zeolite crystal permeability is critical to understanding the mechanisms of transport through MMMs and improve efforts to model and predict the performance of MMMs. Here we present an original analysis to estimate the permeability of LTA zeolites. This is the first analysis quantifying the transport properties of single crystal LTA zeolite as estimated from experimental measurements. We found that LTA nanoparticles have a zeolite crystal permeability that is approximately two orders of magnitude greater than the polymers used for water purification through reverse osmosis. These results highlight the potential of nanosized LTA zeolites for water separation applications.

However, our analysis shows the need for continued research into formation mechanisms of MMMs. With the critical properties of permeability estimated for LTA zeolites, the challenge now is to incorporate them effectively into the polymer matrix. An improved understanding of how zeolite nanoparticles transition from the monomer solution and are incorporated during polymerization in the polyamide matrix will be important to controlling zeolite loading and potential aggregation issues. Reducing or eliminating zeolite aggregation may prove critical to maximizing the potential of LTA zeolites for reverse osmosis.

### **FUNDING**

575

585

595

610

625

This work was supported by a NASA Office of the Chief Technologist's Space Technology Research Opportunity – Early Career Faculty Grant #NNX12AQ45G, the National Science Foundation CAREER Program Award #CBET-1254215, and the Ira A. Fulton Schools of Engineering at Arizona State University.

### **REFERENCES**

- Gude, V.G., N. Nirmalakhandan, and S. Deng, Renewable and sustainable approaches for desalination. Renewable and Sustainable Energy Reviews, 2010. 14(9): p. 2641–2654.
  - Srinivas, V., et al., Reducing energy consumption for seawater desalination. American Water Works Association. Journal, 2007. 99(6): p. 95–106.12.
  - Mulder, M., Basic Principles of Membrane Technology. 2nd Ed. ed1996, Dordrecht, Neth.: Kluwer. 564.
  - 4. Wijmans, J.G. and R.W. Baker, *The Solution-Diffusion Model a Review*. Journal of Membrane Science, 1995. **107**(1-2): p. 1–21.
- Song, Y.J.S., P.; Henry, L. L.; Sun, B. H., Mechanisms of structure and performance controlled thin film composite membrane formation via interfacial polymerization process. Journal of Membrane Science, 2005. 251(1-2): p. 67–79.
  - Jian, K., P.N. Pintauro, and R. Ponangi, Separation of dilute organic/water mixtures with asymmetric poly(vinylidene fluoride) membranes. Journal of Membrane Science, 1996. 117(1-2): p. 117–133.
    - Anderson, M.R.M., B. R.; Reiss, H.; Kaner, R. B., Conjugated Polymer-Films for Gas Separations. Science, 1991. 252(5011): p. 1412–1415.
- 8. Geise, G.M.P., H. B.; Sagle, A. C.; Freeman, B. D.; McGrath, J. E., Water permeability and water/salt selectivity tradeoff in polymers for desalination. Journal of Membrane Science, 2011. 369(1-2): p. 130–138.
  - 9. Robeson, L.M., *The upper bound revisited*. Journal of Membrane Science, 2008. **320**(1-2): p. 390–400.
- 10. Robeson, L.M., Correlation of Separation Factor Versus Permeability for Polymeric Membranes. Journal of Membrane Science, 1991. **62**(2): p. 165–185.
  - 11. Verweij, H., *Inorganic membranes*. Current Opinion in Chemical Engineering, 2012. **1**(2): p. 156–162.
  - Zimmerman, C.M., A. Singh, and W.J. Koros, *Tailoring mixed matrix composite membranes for gas separations*. Journal of Membrane Science, 1997. 137(1-2): p. 145–154.
  - Vu, D.Q., W.J. Koros, and S.J. Miller, Mixed matrix membranes using carbon molecular sieves: I. Preparation and experimental results. Journal of Membrane Science, 2003. 211(2): p. 311–334.
- Breck, D., et al., Crystalline zeolites. I. The properties of a new synthetic zeolite, type A. Journal of the American chemical society, 1956. 78(23): p. 5963–5972.
  - Moore, T.T., et al., Hybrid membrane materials comprising organic polymers with rigid dispersed phases. Aiche Journal, 2004. 50(2): p. 311–321.
- 620 16. Cui, J.Y., et al., Preparation and application of zeolite/ceramic microfiltration membranes for treatment of oil contaminated water. Journal of Membrane Science, 2008. 325(1): p. 420–426.
  - Mosleh, S., et al., Zeolite filled polyimide membranes for dehydration of isopropanol through pervaporation process. Chemical Engineering Research & Design, 2012. 90(3A): p. 433–441.
  - Vatanpour, V., et al., TiO2 embedded mixed matrix PES nanocomposite membranes: Influence of different sizes and types of nanoparticles on antifouling and performance. Desalination, 2012. 292: p. 19–29.
- Dai, Y., et al., Ultem((R))/ZIF-8 mixed matrix hollow fiber membranes for CO2/N-2 separations. Journal of Membrane Science, 2012. 401: p. 76–82.
  - Guan, H.M., et al., Poly(vinyl alcohol) multilayer mixed matrix membranes for the dehydration of ethanol-water mixture. Journal of Membrane Science, 2006. 268(2): p. 113–122.

- Lue, S.J., et al., Diffusivity enhancement of water vapor in poly(vinyl alcohol)-fumed silica nano-composite membranes: Correlation with polymer crystallinity and free-volume properties. Journal of Membrane Science, 2008. 325(2): p. 831–839.
- 22. Sairam, M., et al., *Novel dense poly(vinyl alcohol)-TiO2 mixed matrix membranes for pervaporation separation of water-isopropanol mixtures at 30 degrees C*. Journal of Membrane Science, 2006. **281**(1-2): p. 95–102.
- 23. Jiang, L.Y., et al., Fundamental understanding of nano-sized zeolite distribution in the formation of the mixed matrix single- and dual-layer asymmetric hollow fiber membranes. Journal of Membrane Science, 2005. 252(1-2): p. 89–100.
- 24. Jeong, B.H., et al., *Interfacial polymerization of thin film nanocomposites: A new concept for reverse osmosis membranes*. Journal of Membrane Science, 2007. **294**(1-2): p. 1–7.
- 25. Chmelik, C., et al., *A new view of diffusion in nanoporous materials*. Chemie Ingenieur Technik, 2010. **82**(6): p. 779–804.
- 26. Turgman-Cohen, S., et al., *Molecular Dynamics of Equilibrium and Pressure-Driven Transport Properties of Water through LTA-Type Zeolites*. Langmuir, 2013. **29**(40): p. 12389–12399.
- Pendergast, M.M. and E.M.V. Hoek, A review of water treatment membrane nanotechnologies. Energy & Environmental Science, 2011. 4(6): p. 1946–1971.
- Lind, M.L., et al., Tailoring the Structure of Thin Film Nanocomposite Membranes to Achieve Seawater RO Membrane Performance. Environmental Science & Technology, 2010. 44(21): p. 8230–8235.
- 29. Lind, M.L., et al., *Effect of mobile cation on zeolite-polyamide thin film nanocomposite membranes*. Journal of Materials Research, 2009. **24**(05): p. 1624–1631.
- Mulder, M., Basic principles of membrane technology. 2nd ed1996, Dordrecht; Boston: Kluwer Academic. 564 p.
- Lin, N.H., et al., Polymer surface nano-structuring of reverse osmosis membranes for fouling resistance and improved flux performance. Journal of Materials Chemistry, 2010. 20(22): p. 4642-4652.
- 32. Baker, R.W., Membrane Transport Theory, in Membrane Technology and Applications 2004, John Wiley & Sons, Ltd. p. 15–87.
- Louie, J.S., I. Pinnau, and M. Reinhard, Effects of surface coating process conditions on the water permeation and salt rejection properties of composite polyamide reverse osmosis membranes. Journal of Membrane Science, 2011. 367(1-2): p. 249–255.
- 34. Dalwani, M., et al., Effect of pH on the performance of polyamide/polyacrylonitrile based thin film composite membranes. Journal of Membrane Science, 2011. 372(1-2): p. 228–238.
- 35. Ghosh, A.K. and E.M.V. Hoek, *Impacts of support membrane structure and chemistry on polyamide-polysulfone interfacial composite membranes*. Journal of Membrane Science, 2009. **336**(1-2): p. 140–148.
- Liu, M.H., et al., Thin-film composite membrane formed by interfacial polymerization of polyvinylamine (PVAm) and trimesoyl chloride (TMC) for nanofiltration. Desalination, 2012. 288: p. 98–107.
- 37. Wei, J., et al., Influence of monomer concentrations on the performance of polyamide-based thin film composite forward osmosis membranes. Journal of Membrane Science, 2011. **381**(1-2): p. 110–117.
- 38. Chung, T.S., S.K. Teoh, and X.D. Hu, Formation of ultrathin high-performance polyethersulfone hollow-fiber membranes. Journal of Membrane Science, 1997. 133(2): p. 161–175.
- 39. de Vos, R.M. and H. Verweij, *High-selectivity, high-flux silica membranes for gas separation.* Science, 1998. **279**(5357): p. 1710–1711.
- 40. Kawakami, H., M. Mikawa, and S. Nagaoka, *Gas permeability and selectivity through asymmetric polyimide membranes*. Journal of Applied Polymer Science, 1996. **62**(7): p. 965–971.
- Kusakabe, K., et al., Formation of a Y-type zeolite membrane on a porous alpha-alumina tube for gas separation. Industrial & Engineering Chemistry Research, 1997. 36(3): p. 649–655.
- 42. Xu, X.C., et al., Synthesis of a high-permeance NaA zeolite membrane by microwave heating. Advanced Materials, 2000. 12(3): p. 195-+.
- 43. Guillen, G.R., et al., Pore-structure, hydrophilicity, and particle filtration characteristics of polyaniline-polysulfone ultrafiltration membranes.
   700 Journal of Materials Chemistry, 2010. 20(22): p. 4621–4628.

640

645

650

655

675

685

690

- 44. Li, W.X., W.H. Xing, and N.P. Xu, *Modeling of relationship between water permeability and microstructure parameters of ceramic membranes*. Desalination, 2006. **192**(1-3): p. 340–345.
- 45. Chakrabarty, B., A.K. Ghoshal, and M.K. Purkait, SEM analysis and gas permeability test to characterize polysulfone membrane prepared with polyethylene glycol as additive. Journal of Colloid and Interface Science, 2008. 320(1): p. 245–253.
- 46. Pinnau, I., et al., Gas Permeation through Composite

  Membranes. Journal of Membrane Science, 1988. 37(1): p.
  - 47. Henis, J.M.S. and M.K. Tripodi, *Composite Hollow Fiber Membranes for Gas Separation the Resistance Model Approach*. Journal of Membrane Science, 1981. **8**(3): p. 233–246.
- 715 48. Louie, J.S., et al., Effects of polyether-polyamide block copolymer coating on performance and fouling of reverse osmosis membranes. Journal of Membrane Science, 2006. 280(1-2): p. 762–770.

49. Hashemifard, S.A., A.F. Ismail, and T. Matsuura, *A new theoretical gas permeability model using resistance modeling for mixed matrix membrane systems*. Journal of Membrane Science, 2010. **350**(1-2): p. 259–268.

720

725

730

- 50. Pope, C., *Nucleation and growth theory in zeolite synthesis*. Microporous and mesoporous materials, 1998. **21**(4): p. 333–336.
- 51. Soroush, A., et al., *Interfacially polymerized polyamide thin film composite membranes: Preparation, characterization and performance evaluation*. Desalination, 2012. **287**(0): p. 310–316.
- 52. Dong, H., et al., *Preparation and characterization of surface-modified zeolite-polyamide thin film nanocomposite membranes for desalination*. Desalination and Water Treatment, 2011. **34**(1-3): p. 6–12.
- 53. Dong, G., H. Li, and V. Chen, *Challenges and opportunities for mixed-matrix membranes for gas separation*. Journal of Materials Chemistry A, 2013. **1**(15): p. 4610–4630.
- 54. Merkel, T.C., et al., *Ultrapermeable, Reverse-Selective Nanocomposite Membranes*. Science, 2002. **296**(5567): p. 519–522.